DNA Origami Nanoarrays for Multivalent Investigations of Cancer Cell Spreading with Nanoscale Spatial Resolution and Single-Molecule Control

Da Huang,[†] *Ketan Patel,*[‡] *Sandra Perez-Garrido,*[†,‡] *John F. Marshall,*[‡,*] *and Matteo Palma*[†,*]

† School of Biological and Chemical Sciences, Materials Research Institute, and Institute of Bioengineering, Queen Mary University of London, Mile End Road, London E1 4NS, United Kingdom

‡ Barts Cancer Institute, Cancer Research UK Centre of Excellence, Queen Mary University of London, Charterhouse Square, London EC1M 6BQ, United Kingdom

KEYWORDS: multivalency; cooperativity; DNA nanotechnology; cancer cell; single-molecule; biomimetic nanoarrays; spatial control.

ABSTRACT

Here we present a strategy for the fabrication of biomimetic nanoarrays, based on the use of DNA origami, that permit the multivalent investigation of ligand-receptor molecule interactions in cancer cell spreading, with nanoscale spatial resolution and single-molecule control. We employed DNA-origami to control the nanoscale spatial organization of integrin- and epidermal growth factor (EGF)- binding ligands that modulate epidermal cancer cell behaviour. By organizing these multivalent DNA nanostructures in nanoarray configurations on nanopatterned surfaces, we demonstrated the cooperative behaviour of integrin- and EGF- ligands in the spreading of human cutaneous melanoma cells: this cooperation was shown to depend on both the number and ratio of the selective ligands employed. Notably, the multivalent biochips we have developed allowed for this cooperative effect to be demonstrated with single-molecule control and nanoscale spatial resolution. By and large, the platform presented here is of general applicability for the study, with molecular control, of different multivalent interactions governing biological processes, from the function of cell-surface receptors, to protein-ligand binding and pathogen inhibition.

Cells interact with the extracellular matrix (ECM) *via* transmembrane proteins called integrins: integrin-mediated interactions with the ECM control cell adhesion, migration and invasion,[1,2] and play a central role in cancer.[3] Notably, integrins work in concert with other membrane receptors to modulate normal and cancer cell behaviour,[4-6] but the combined spatial organization and stoichiometry required are not known. Studying these relationships at the nanoscale is a significant challenge as current strategies do not allow for combined multivalence capability and nanoscale spatial control; this in turn represents a barrier to our understanding of the fundamental mechanisms by which receptor crosstalk dictates cell behaviour, including metastasis.

Various approaches have been pursued to control the spatial organization of cellular adhesion receptors on surfaces[7-13] in order to understand the ECM geometries that affect cell spreading and focal contact formation,[14-17] and to develop functional integrin complexes.[18,19] Among these works, the most notable in terms of single-integrin control, as well as nanoscale spatial resolution, are based on the use of metal nanodots employed as anchoring points for cell-binding peptides, and the consequent fabrication of ECM biomimetic nanoarrays.[12,13,20-23] In this context, micellar diblock copolymer self-assembly demonstrated that a preferential spacing of ~60nm between integrin binding sites is key for efficient cell spreading and viability;[10,24] this approach further allowed investigating optimal substrate rigidity for adhesion formation as a function of ligand spacing.[8] Additionally, a nanolithographic strategy was employed to fabricate nanoscale bio-arrays that showed the importance of integrin clustering: the juxtaposition within 60 nm of at least 4 cell-adhesion peptide-liganded integrins was shown to be required for the establishment of stable focal adhesions.[11] A similar approach was used to further employ this platform in bifunctional configurations.[25] However, while these approaches shed light on the importance of the nanoscale geometrical arrangement of integrin-binding peptides in ECM-mimicking substrates, they do not

allow for combined multivalence capability and nanoscale spatial resolution toward the targeting of different, and synergistic, cell receptors with single-molecule control.

Here we report a strategy for the fabrication of biomimetic nanoarrays that permit the investigation of multivalent ligand-receptor molecule interactions in cell spreading, with nanoscale spatial resolution and single-molecule control. In particular, we combined the ability of DNA-origami to control the nanoscale spatial organization[26-32] of distinct cell-binding ligands, with our recently developed Focused Ion Beam (FIB) patterning procedure to assemble functional DNA nanostructures on surfaces in array configurations.[33] This allowed us to fabricate reusable biomimetic substrates and, as a proof of concept, study integrin-dependent responses and their cooperation with epidermal growth factor (EGF)[34-36] that modulate epidermal cancer cell behaviour. A cooperative behaviour in the spreading of human cutaneous melanoma cells was demonstrated when both integrin- and EGF-binding ligands were assembled in the biomimetic nanoarrays. Additionally, this cooperation was shown to depend on both the number and ratio of the selective ligands employed and assembled with nanoscale spatial control.

RESULTS AND DISCUSSION

We engineered triangular DNA origami nanostructures with both the integrin αvβ6-specific 20-mer peptide A20FMDV2[37] and EGF (see Figure 1a). A20FMDV2 was chosen as it was found to bind more selectively to αvβ6 integrins, an integrin family that is overexpressed in specific types of cancers: approximately one-third of carcinomas express αvβ6.[38] EGF was employed as integrins work co-operatively with receptor tyrosine kinases[39-41] to modulate cell behaviour: the reported activities of integrins and receptor tyrosine kinases on cancer cell behaviour and cancer development[42] are likely to have been a product of functional co-regulation of these two receptor families.[43]

The A20FMDV2 peptide was first conjugated to a ssDNA[44] (see the Supporting Information (SI) and Figure S1). The conjugation was performed *via* maleimide-thiol strategy on the C-terminal cysteine modification of A20FMDV2 and the maleimide-modified ssDNA, and the conjugation products were validated and purified *via* size exclusion high-performance liquid chromatography (HPLC, see Figure S2a): the yield of conjugation was calculated to be of ca 63% (see the SI). The DNA-peptide conjugates were then assembled on the DNA nanostructures *via* in-solution hybridization with the complementary ssDNA "sticky-ends" present on the DNA origami by design (see Figure S1); the number and position of the peptides per DNA origami were controlled by the number and position of the sticky ends designed in the pristine DNA-origami. A 6-peptide modified DNA origami nanostructure was achieved at first and analysed by polyacrylamide gel electrophoresis (Figure S2b), confirming the presence of the peptide on the DNA-origami after hybridization. We designed the DNA origami to exhibit 60nm spacing between the A20FMDV2 peptides, in line with the preferential spacing of ~60nm between integrin binding sites shown to be key for efficient cell spreading and viability[10,24] as well as for the establishment of stable focal adhesions.[11]

For the modification of the DNA-origami with EGF, biotin modified sticky ends were designed on the DNA nanostructures (see Figure S1) so to then bind streptavidin conjugated EGFs (see the SI and Figure 1a). In order to co-localize both the A20FMDV2 and EGF on the modified DNA origami system, the assembly of the EGF-streptavidin conjugate was performed on the previously constructed A20FMDV2 modified DNA nanostructures, employing biotinylated sticky ends which differ in position from the A20FMDV2 modified ones (see Figure 1a). The assembled nanostructures were further validated by Atomic Force Microscopy (AFM) imaging by casting diluted solutions on muscovite mica substrates (Figure 1b). The streptavidin-modified EGFs are

clearly visible under AFM and were revealed to be around 5 nm in height, in agreement with their size when cast pristine on mica. Notably, the yield of EGF modification was found to be up to 87%.

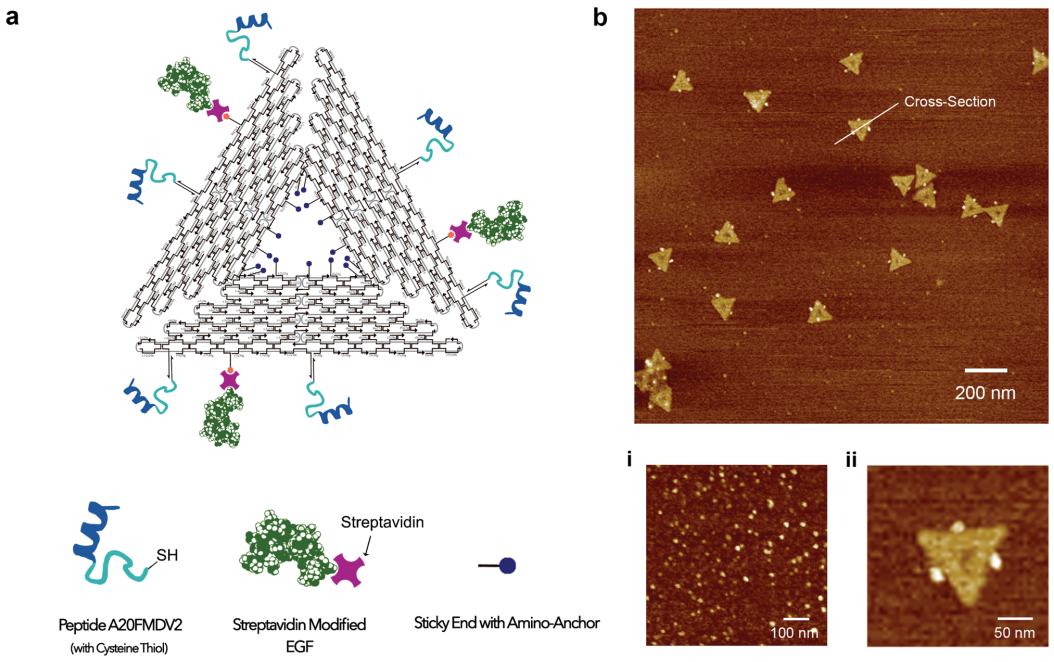

Figure 1. (a) Schematic of modifying EGF and A20FMDV2 peptide on triangular DNA origami. (b) AFM images of EGF modified DNA origami. i) The EGF by itself scanned under AFM is shown. ii) The zoom-in AFM image of EGF modified origami.

In order to organize on surfaces the A20FMDV2- and EGF-modified DNA origami in array configurations, we covalently immobilized them on patterned arrays fabricated employing our recently developed FIB strategy.[33,45] Highly uniform nanoarrays can be formed with a one-step lithographic process on metal-coated glass SiO_2 surfaces; apertures matching the size of the DNA origami employed were patterned, and the exposed glass substrate was functionalized with carboxylic-terminating silane (see Figure S3). This allowed us to covalently bind on these apertures our DNA-origami pre-designed to exhibit amino-terminating ssDNA employed as

anchoring moieties for surface immobilization (see Figure S3). Figure 2a shows AFM images demonstrating the selective placement of ligand-modified DNA origami in the patterned nanoapertures, *via* the covalent immobilisation approach on the exposed SiO_2 surface: a high yield of 82% ± 0.17 over arrays of 64 μm^2 can be achieved for the one-to-one immobilisation of DNA origami per nanoaperture.

The controlled nanoscale arrangement of the functional ligands (A20FMDV2 and/or EGF) on the DNA nanostructures, combined with the aforementioned patterning strategy, allowed us to fabricate arrays of multi-ligand functionalized DNA-origami. A spacing of 60nm between ligands was chosen as this was proven to be the ideal spacing between integrin binding sites for efficient cell spreading and viability.[11,15,20] Additionally, a 300 nm spacing per nanoaperture, and hence per DNA origami, was chosen as the standard spacing for the nanoarrays in order to achieve a density of at least 87 ligands per μm^2 (See Figure S4)[46]. The substrates were then employed as multivalent ECM-mimicking biochips for cell adhesion and spreading investigations: Figure 2b shows a schematic of the typical experimental set-up.

In our studies we employed an isogenic pair of human melanoma cell lines (A375Ppuro and A375Pβ6) that differed only in their expression of integrin αvβ6. Differences in the binding of the αvβ6-positive A375Pβ6 cells compared with the binding of the αvβ6-negative A375Ppuro cells can therefore be taken as an indication of the binding activity of the αvβ6 integrins. It should be noted, that although the isogenic pair was used as a model for αvβ6-dependent binding, both cell lines are able to respond to EGF.[47-49] Thus, the biological responses of different receptor classes on cells binding to different ligand classes can be investigated; this can be achieved with single molecule control (one ligand per integrin/EGF) and nanoscale spatial resolution, by employing the multivalent platform developed here.

All patterned substrates were blocked with 1% BSA prior to cell plating in order to reduce the nonspecific adhesion, and only expose the patterned ligands. Plain patterned substrates without any DNA immobilised on the surface were employed as blank control samples, while non-modified origami immobilised on the substrates were used as another set of control samples (*i.e.* with origami that did not exhibit any ligands). Moreover, both types of cells were also plated on plain glass coverslips saturated with binding sites (see the experimental section), employed as positive control samples. The same numbers of cells were plated on each substrate and incubated for 1.5 hours. Careful PBS washing was carried out after cell incubation, and the substrates were then imaged under differential interference contrast microscopy (DIC).

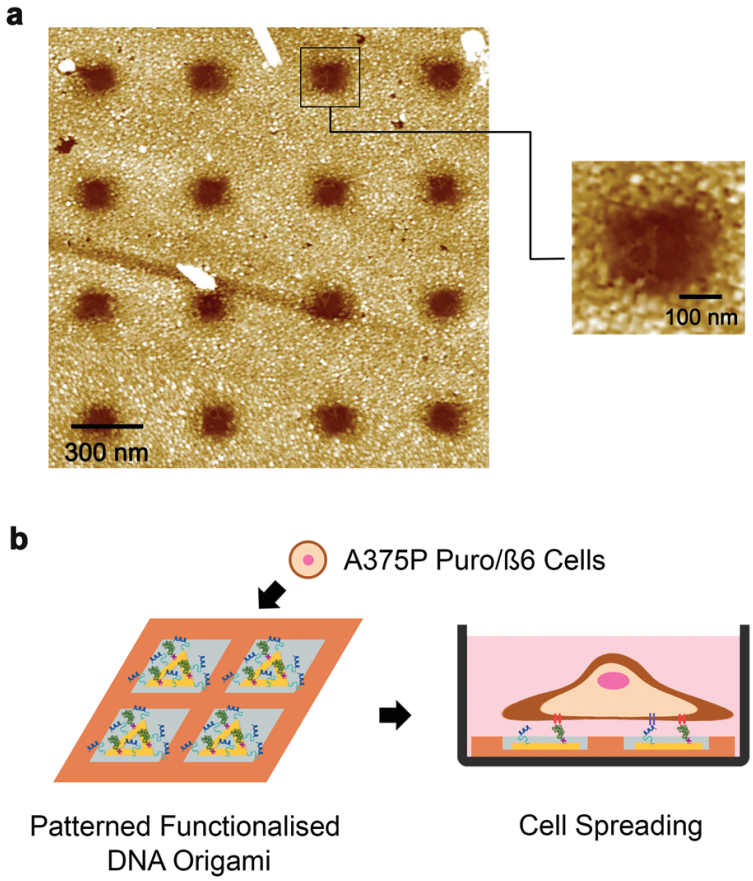

Figure 2. (a) Representative AFM image of the assembly of DNA origami in nanoarrays *via* covalent immobilisation in pre-patterned nanoapertures: the zoom-in AFM image shows one origami in the nanoaperture; (b) schematic of cell spreading studies on patterned functionalised DNA origami.

Figure 3a-i shows DIC images of A375P cells (both A375Ppuro and A375Pβ6 cells) on substrates nanopatterned with triangular DNA origami containing six A20FMDV2 peptides each (see the experimental section). The substrates engineered with the DNA origami containing the peptides induced a higher degree of A375Pβ6 cell spreading (up to 63 ± 5.3 %) compared to those on blank patterned and plain origami functionalised slides (approximately 1%): see Figure 3a-ii. Notably, on the peptide modified substrates, the A375Ppuro cells exhibited a lower spreading degree compared to A375Pβ6 cells, likely due to αvβ6 integrin expression only on the A375Pβ6 cells. Additionally, plain DNA origami nanostructures were revealed to promote no binding of either cell types (approximately 1%). These data indicate that cell spreading relied only on cell attachment to the A20FMDV2 peptides.

Cell spreading studies were then performed employing DNA origami substrates modified with both A20FMDV2 peptides and EGF (both ligands arranged on each DNA-origami, that in turn were organized in arrays). Substrates modified with only A20FMDV2 peptides, and ones modified with only EGF, were also tested as control samples in order to reveal the independent binding properties of these two ligands: this comparison would highlight the cooperative nature of the two ligands. Because we employed an EGF-streptavidin-biotin conjugation approach to modify the DNA origami with EGF, streptavidin-only modified substrates were also used as controls to rule out any potential active role of streptavidin in cell binding. Moreover, plain patterned substrates without any DNA, and plain glass coverslips were employed as usual as blank controls and positive

controls: the blank control did not present any cell-binding ligands, while the positive control was saturated with cell-binding ligands. A375Pβ6 and A375Ppuro cells were plated onto all these substrates; cell spreading investigations were then performed *via* DIC (see Figures 3b-i), and the cell spreading numbers and areas (assessed *via* ImageJ), indicating the cell spreading level, were quantitatively analyzed as percentages compared to the positive control samples saturated with cell-binding ligands[11,20] (Figure 3b-ii).

On substrates modified with both ligands (with a density of 87 peptides/μm^2 and 44 EGF molecules/μm^2), the A375Pβ6 cells showed a significantly higher percentage of spreading (77% ±6.3, $p<0.05$) compared to spreading onto A20FMDV2 peptide-only substrates (57% ±4.7) and EGF-only substrates (35% ±5.1). Differently, the A375Ppuro exhibited only 6% ±1.2 spreading onto A20FMDV2 peptides-only substrate, but showed 42% ±4.9 spreading to the EGF-only origami, and 47% ±5.8 to the A20FMDV2/EGF-expressing origami. These data suggest the enhanced spreading exhibited by A375Pβ6 in the double ligand-coated origami is due to the expression of αvβ6. Additionally, Streptavidin modified substrates showed negligible cell spreading (3% for A375Ppuro cells and 4% for A375Pβ6 cells), indicating that streptavidin does not affect cell binding. Notably, for A375Pβ6 cells, there was a higher spreading cell behaviour (75% ±6.5, $p<0.05$) observed on substrates modified with both ligands, while for A375Ppuro cells the spreading in the presence of both ligands was found to be just below 50%.

These results suggest that both A20FMDV2 peptides and EGF exhibit a positive effect on the establishment of spreading for A375Pβ6 cells. While A20FMDV2-substrates showed selective binding of A375Pβ6 but not of A375Ppuro cells, EGF was positive to both A375Pβ6 and A375Ppuro cells: the cooperative effect of the A20FMDV2 and EGF ligands is highlighted by the

promotion of cell spreading for both cell types. It is important to remark that a boost in cell spreading was observed especially for A375Pβ6 cells: 77% for ß6 compared to 47% for A375Ppuro. This strongly suggest that both types of ligands need to be present for the establishment of a significant yield of spreading for A375Pβ6 cell lines (Figure 3b-iii).

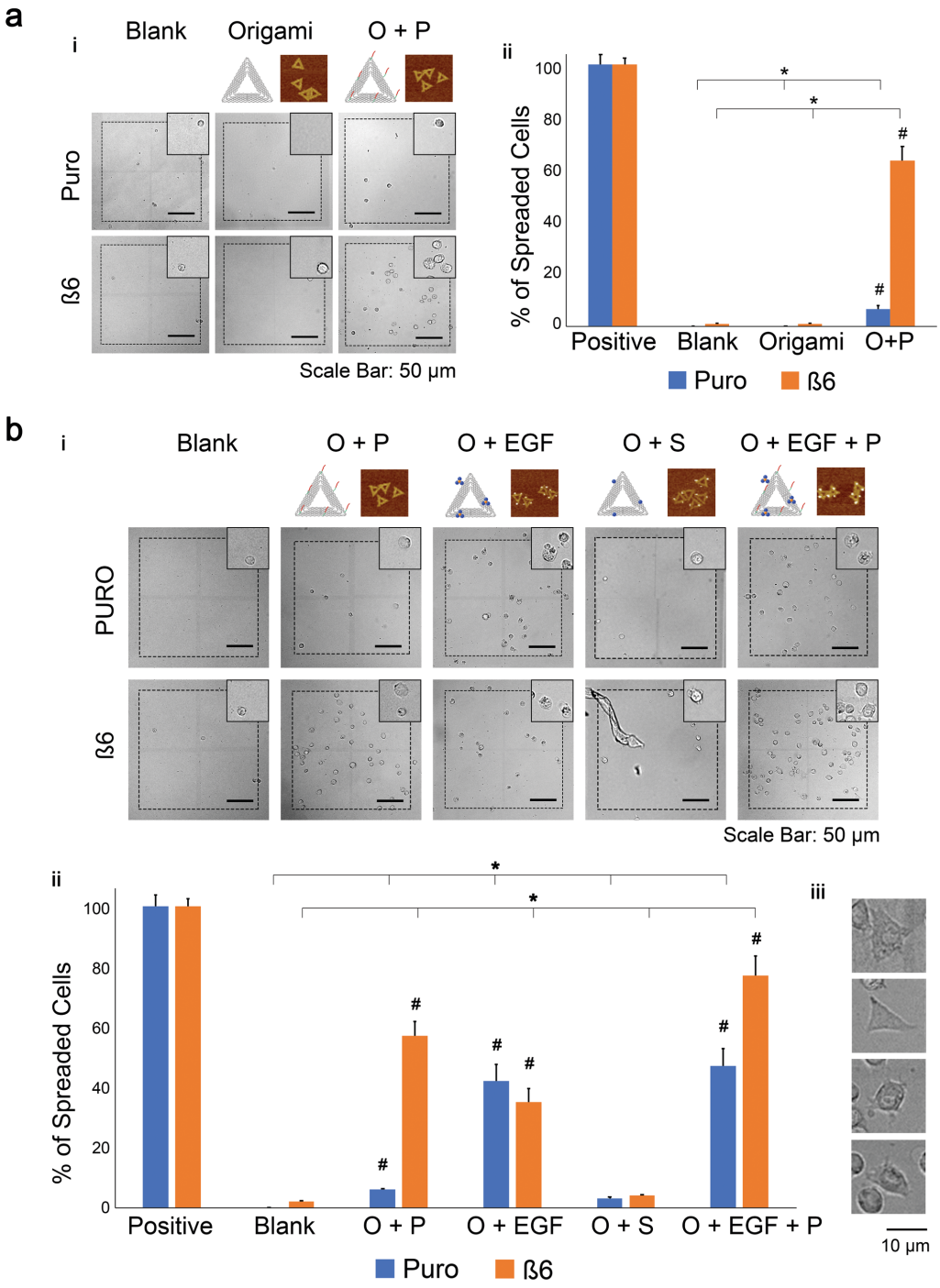

Figure 3. (a) A375Ppuro (blue) and A375Pβ6 (orange) cell spreading study on patterned DNA origami substrates with 300 nm spacing: i) DIC images of cell spreading on different substrates (positive control, blank, plain origami, and O+P (peptide assembled origami)) with 4× zoom-in

insert images; ii) quantitative analysis of cell spreading on each substrate. The percentage of adherent cells compared to positive control and standard errors are shown. A promotion of A375Pβ6 cells spreading was shown on the peptides modified origami substrate (63%) ($^{\wedge}p < 0.05$ vs. positive control sample, and $^{*}p < 0.05$ vs. O+P sample group). (b) A375Ppuro and A375Pβ6 cell spreading study on substrates modified with both A20FMDV2 peptide and EGF: i) DIC images of cells spreading on different substrates (positive control, blank, O+P (peptide assembled origami), O+EGF (EGF assembled origami), O+S (Streptavidin assembled origami), and O+EGF+P (both peptide and EGF assembled origami)) with 4× zoom-in insert images; ii) quantitative analysis of cell spreading on each substrate. The percentage of adherent cells compared to the positive control, and the standard errors are shown. iii) Zoom-in DIC images of A375Pβ6 cell spreading on DNA origami substrates modified with both A20FMDV2 and EGF: a high level of spreading was shown. ($^{\#}p < 0.05$ vs. positive control sample, and $^{*}p < 0.05$ vs. O+EGF+P sample group).

In order to further investigate the cooperation between A20FMDV2 and EGF, we varied the ratio between the two ligands in each DNA origami and investigated the cell spreading of the A375P cell line. DNA nanostructures exhibiting different combinations were assembled by modifying specific staple strands at selected positions on the DNA origami: we employed ratios of peptide to EGF of 1:1, 1:3, 3:3, 3:6, 3:1 and 6:3. Both A375Ppuro and A375Pβ6 cells were plated on the different multivalent nanoarray chips; their spreading was investigated *via* DIC imaging (Figure 4a). A quantitative analysis of the percentage of adhering cells and cell areas was calculated for each experiment: Figure 4b summarizes the results obtained.

For all ratios, the spreading of A375Pβ6 cells were shown to be above 50% when both EGF and A20FMDV2 were present on the DNA-origami nanoarray. Additionally, we observed a A375Pβ6

cell spreading efficiency above 60% when at least 3 A20FMDV2 (P) peptides were present per DNA-origami. In particular, we found this spreading efficiency to range between 66% ±6.0 and 78% ±6.3, depending on the number of concomitant EGF (E) on the DNA-nanostructure. In this regard, the spreading increased with the higher number of EGF per DNA nanostructure: from 66% ±6.0 (for a ratio P:E=3:1) to 71% ±5.7 (for P:E=3:3), and 78% ±6.3 (for P:E=3:6) ($p<0.05$). The best yield for ß6 cell spreading was therefore observed for the combination Peptide:EGF(P:E) with a ratio of 3:6, resulting in 78% spreading efficiency (see Figure 4b); this result is also corroborated by the cell area analysis: see Figure 4b-ii.

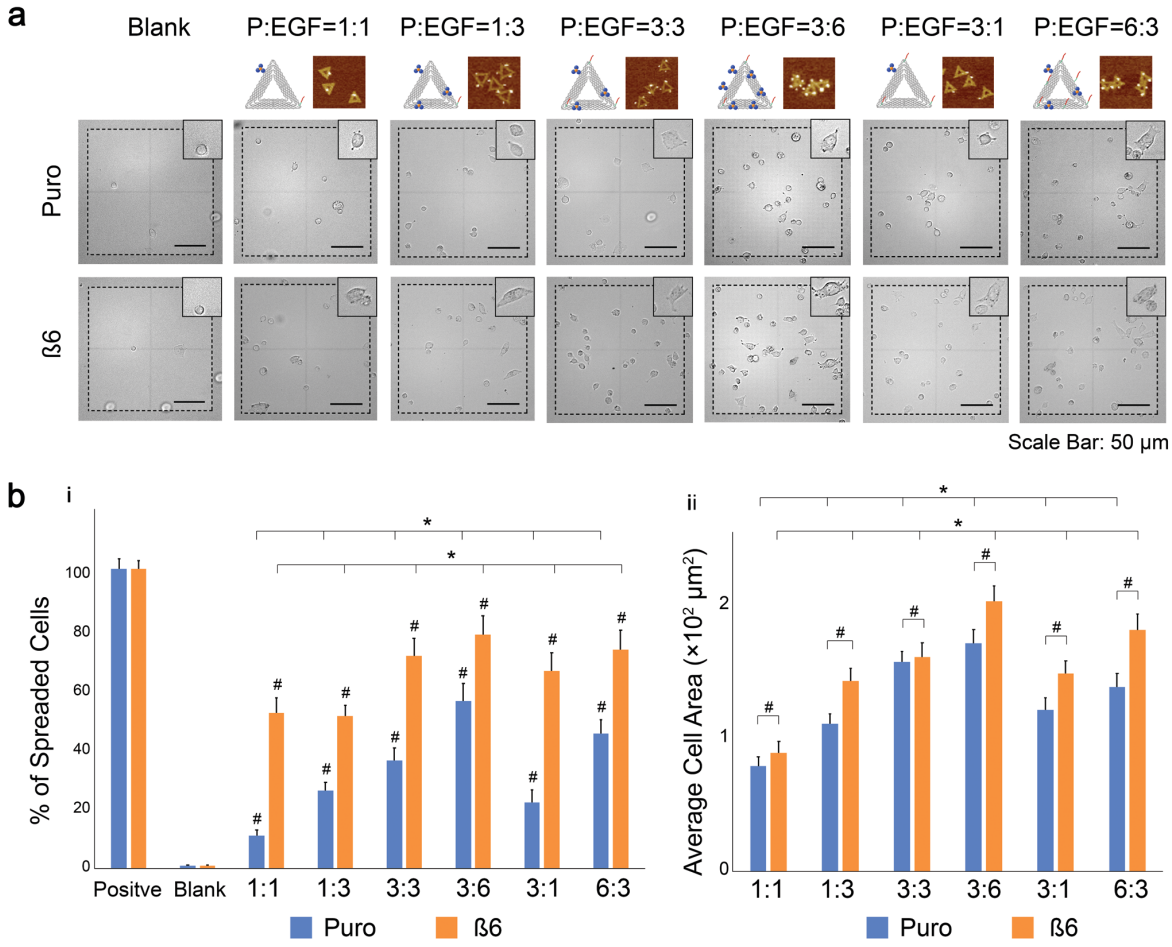

Figure 4. Study of the cooperation between the peptide and EGF as a function of their ratio from 1:1 to 6:3. (a) A375Ppuro and A375Pβ6 cell spreading study on patterned DNA origami substrates

with different combination of A20FMDV2 peptide to EGF: 1:1, 1:3, 3:3, 3:6, 3:1 to 6:3: DIC images of cell spread on different substrates with 4× zoom-in insert images. Modified origami models and AFM characterisations are shown; (b) quantitative analysis of cell spreading on each substrate; i) the percent of adherent cells compared to positive control are shown with standard errors; the increase of EGF favours spreading of A375Pβ6 cells, while the presence of at least 3 peptides increases spreading above 65% (and up to 78%): the best ratio for cell spreading was found to be Peptide:EGF=3:6. ($^{\#}p < 0.05$ vs. positive control sample, and $*p < 0.05$ vs. between different sample groups); ii) the average cell area counting was analysed which corroborated to the spreading analysis ($^{\#}p < 0.05$ vs. between each same condition of A375Ppuro and A375Pβ6 cell, and $*p < 0.05$ vs. between different sample groups, assessed *via* ImageJ).

CONCLUSIONS

In this work, we presented a strategy for the fabrication of biomimetic nanoarrays that permit the investigation of multivalent ligand-receptor molecule interactions in cell spreading, with nanoscale spatial resolution and single-molecule control. The substrates were patterned using DNA origami organized in arrays and modified to exhibit cell-adhesion ligands spaced 60nm apart: A20FMDV2 peptides and EGF were the two ligands investigated here, because of their known roles in binding to the ligand receptors on human melanoma cell lines. We investigated the attachment and spreading of an isogenic pair of human melanoma cell lines (A375Ppuro and A375Pβ6) that differed only in their expression of integrin αvβ6, an integrin family that is overexpressed in specific types of cancers: approximately one-third of carcinomas express αvβ6. The data show that both cell types bound equally well to EGF-labelled origami, whereas binding to A20FMDV2 was almost exclusively by A375Pβ6 cells. We found that A20FMDV2 and EGF

exhibit a positive cooperation in promoting the spreading of A375Pβ6 cells. An increase in the spreading efficiency was observed with increasing number of ligands, in line with A20FMDV2's selective binding to αvβ6 integrins, and its cooperation with EGF.[39-41] Moreover, we found that the presence of at least 3 peptides in the system, hence 3 integrins per cluster, favors maximum attachment, while the best ratio for cell spreading was found to be Peptide:EGF=3:6. To the best of our knowledge, the multivalent platform we have developed allowed for this cooperative effect to be demonstrated with single-molecule control and nanoscale spatial resolution. This methodology will allow us to dissect, in future studies, the stoichiometry of receptor interactions and the consequential signaling pathways that regulate both normal and cancer cell behavior, with molecular control. Additionally, the platform we presented here is of general applicability for the study, with nanoscale spatial control and single-molecule resolution, of different multivalent interactions governing biological processes,[50] from the function of cell-surface receptors[51] to ligand-protein binding[30] and pathogen inhibition.[52]

METHODS

Synthesis of DNA Origami: DNA origami is assembled by combining M13mp18 (5 nM) and staple strands (50 nM) in 50 μL TAE buffer with 12.5 mM Mg^{2+} (See DNA sequences in supporting information: Table S1 and S2). M13mp18 is a bacteria phage vector strand with 7249 bases long. An appropriate quantity of ions, such as magnesium here or sodium in the DNA hybridisation approach, are demanded to equilibrate the electrostatic repulsion between highly negatively charged DNAs molecules. An amount of 12.5 mM Mg^{2+} was chosen based on balancing the increase of the yield and reduction of the aggregation. The mixture solution is heated to 94°C to completely dihybridise all of dsDNA. Temperature step controlled cooled down approach is

carried out in a PCR machine. From 94°C to 65°C, cooling rate is about at 0.3°C per minute. A cooling rate of 0.1°C per minute is employed from 65°C to room temperature. The self-assembled DNA origami is purified with Millipore Amicon Ultra 100 kDa spin columns in a centrifuge at 13000 rpm for 2 minutes, 3 times, to get rid of access staple strands. Residues in the spin column is adjusted to a concentration around 20 nM by regulating the volume to about 50 μL. A NanoDrop Spectrophotometer is used to detect the rough concentration of DNA origami products based on the constant of a molecular weight of 330 g/mol per base and an extinction coefficient = 33 mg/ml for A260 = 1. The actual result is normally close to the estimated numbers.

AFM Characterisation of DNA Origami: AFM was used to image the DNA origami structures. DNA origami is cast on either silicon dioxide, glass or mica surfaces for imaging. The DNA origami solution is diluted by TAE buffer with 30 mM Mg^{2+} to around 1nM in order to get a good separation of the DNA nanostructures once immobilised on surface. Magnesium is required in the procedure as an ion charged bridge, immobilising DNA origami to the substrate surfaces. Mica samples were cleaved twice by solid scotch tape immediately prior casting. 5 μL of diluted DNA origami solution was directly deposited on freshly cleaned mica and left to adsorb on the surface for 2 min. Subsequently, the substrate was washed by distilled water to remove non-absorbed origami and then blown dry by compressed air. ScanAsyst-Air tips with 0.4 N/m spring constant were used to scan the sample by AFM under ScanAsyst™ Mode. A resolution of 512 pixels per line with 1 Hz scan rate was chosen for appropriate imaging of the DNA nanostructure.

Modifications of DNA Origami: Peptide A20FMDV2 was assemble on DNA origami using the Maleimide-Thiol linkage on ssDNA complimentary to sticky-ends. The numbers of peptides on a single origami depends on how many complementary sticky-ends that origami has. Up to six positions were chosen in this study (namely at A32, B32 C32, A37, B37, and C37 of a triangular

DNA origami, see SI). Commercially available protected maleimide modified ssDNA need to be deprotected before conjugation. 50 nmoles of the protected maleimide modified ssDNA was freeze dried at first. Deprotection and conjugation will inefficient in the presence of water. Freeze dried samples were washed adding 2 mL of anhydrous acetonitrile, and the solvent was evaporated by a rotary evaporator. 2 mL of anhydrous toluene was added to the vial, mixed and then evaporated. The rinsing procedure was repeated for 3 times. In the third time, toluene was kept in vial and incubated at 90°C for 4 hours to deprotect the maleimide-modifier. After incubation, toluene was evaporated. The vial containing the deprotected maleimide modified ssDNA was immediately mixed with the reduced peptide. The thiol group on the cysteine of the peptide needed to be reduced from the oxide form right before conjugation. The conjugation reaction occurs after the mixing. The mixture was put on a shaker for 1 hour to complete the conjugation. Peptide-ssDNA conjugation was validated and purified by reversed phase HPLC. Purified products were freeze dried and resuspended in TAE buffer. Peptide-ssDNA conjugation was mixed with staple strands and M13mp18, and standard DNA origami synthesis was carried out. A20FMDV2 is a linear peptide with 21 amino acid. Heating up to 94°C will not affect the structure and function of this peptide. Epidermal growth factor (EGF) was modified on DNA origami *via* streptavidin-biotin conjugation. The EGF was biotinylated and assembled with streptavidin which is commercially available. Streptavidin modified EGF was attached on origami structure *via* incubating with DNA origami solution which have biotinylated sticky ends. AFM characterisation was carried out to confirm the EGF modification.

DNA Origami Patterning: DNA origami was patterned on FIB nanofabricated coverslip substrate. DNA origami was first diluted 20 times in Tris buffer (5 mM; pH 8.2) with 30mM Mg^{2+}. 60 μL of the DNA origami solution was cast on the substrate and placed in a 6-wells plate with

moist Kimwipe. The sample was incubated for 90 minutes on a shaker. The sample was then washed with Tris buffer (5 mM; pH 8.2) with 30 mM Mg^{2+} (60 µL × 8). A 0.01% solution of carboxyethylsilane in the same Tris buffer was washed in with (60 µL × 8), and the sample was incubated for 2 minutes on a shaker. The buffer was then exchanged for MOPS buffer (10 mM; pH 8.1) with 30 mM Mg^{2+} (60 µL × 8). An equal volume of EDC (1-Ethyl-3-(3-dimethylaminopropyl) carbodiimide; 50 mM) and NHS (N- hydroxysulfosuccinimide; 100 mM) in the MOPS buffer was added to the sample's volume and the sample was incubated for 10 minutes on a shaker. The sample was washed with the MOPS buffer, then rinsed with DPBS with 125 mM NaCl to remove any uncovalently bound structures, and subsequently rinsed with water. The samples were checked under AFM.

Cell Spreading Study: Cells were grown at 37°C and 8% (v/v) carbon dioxide/air condition in a humidified incubator. Cells were maintained as adherent monolayers on tissue culture plastic. Growth medium contained of DMEM accompanied with 10% FBS. Cells were sub-cultured approximately every three days. After incubation with 0.25% (w/v) trypsin/EDTA solution, adhered cells were removed from culture plastic and neutralised by adding three folds of growth medium. Cells were then suspension to fresh tissue culture flasks with fresh growth medium. Cells were removed from tissue culture plastic by trypsin, and neutralised, pelleted and resuspended as described before. The cell concentrations were counted using cytometer for both Puro and ß6 cell lines. Same numbers of cells for both cell lines were applied on different pattern modified substrate in 24 wells plate. The substrates were blocked with 1% BSA before cells plating. 2 mL of growth medium were added to each well and then incubated for 1.5 hours. The substrates were carefully washed by PBS for 2 times to remove non-adhered cells. The patterned area with cells were imaged using differential interference contrast microscopy (DIC) to observe the cell behaviours. ImageJ

was used for the cell numbers counting and average cell area analysis. The cell images were first threshold and the outline of cells were drawn manually. The entire cell areas were then calculated *via* the software and divided by the cell numbers.

ASSOCIATED CONTENT

Supporting Information

The Supporting Information is available free of charge *via* the Internet at http://pubs.acs.org. Detailed information on the applied synthesis and modifications of DNA origami, sequences information of DNA origami, FIB surface patterning and pattern densities screening (PDF).

AUTHOR INFORMATION

Corresponding Authors

j.f.marshall@qmul.ac.uk

m.palma@qmul.ac.uk

Author Contributions:

The manuscript was written through contributions of all authors. All authors have given approval to the final version of the manuscript.

ACKNOWLEDGMENTS

D.H. was financially supported by the Chinese Scholarship Council. J.F.M acknowledges funding by the BCI Cancer Research UK Centre Award. We further gratefully acknowledge financial support from Queen Mary University of London.

REFERENCES

(1) Gumbiner, B. M. Cell Adhesion: The Molecular Basis of Tissue Architecture and Morphogenesis. *Cell* **1996**, *84*, 345–357.

(2) Zamir, E.; Geiger, B. Components of Cell-Matrix Adhesions. *J. Cell Sci.* **2001**, *114*, 3577–3579.

(3) Hirohashi, S.; Kanai, Y. Cell Adhesion System and Human Cancer Morphogenesis. *Cancer Sci.* **2003**, *94*, 575–581.

(4) Humphries, J. D.; Byron, A.; Humphries, M. J. Integrin Ligands at a Glance. *J. Cell Sci.* **2006**, *119*, 3901–3903.

(5) Wozniak, M. A.; Modzelewska, K.; Kwong, L.; Keely, P. J. Focal Adhesion Regulation of Cell Behavior. *Biochim. Biophys. Acta - Mol. Cell Res.* **2004**, *1692*, 103–119.

(6) Hood, J. D.; Cheresh, D. A. Role of Integrins in Cell Invasion and Migration. *Nat. Rev. Cancer* **2002**, *2*, 91–100.

(7) Karimi, F.; O'Connor, A. J.; Qiao, G. G.; Heath, D. E. Integrin Clustering Matters: A Review of Biomaterials Functionalized with Multivalent Integrin-Binding Ligands to Improve Cell Adhesion, Migration, Differentiation, Angiogenesis, and Biomedical Device Integration. *Adv. Healthc. Mater.* **2018**, *7*, 1701324.

(8) Oria, R.; Wiegand, T.; Escribano, J.; Elosegui-Artola, A.; Uriarte, J. J.; Moreno-Pulido, C.; Platzman, I.; Delcanale, P.; Albertazzi, L.; Navajas, D.; Trepat, X.; García-Aznar, J.;

Cavalcanti-Adam, E.; Roca-Cusachs, P.; Force Loading Explains Spatial Sensing of Ligands by Cells. *Nature* **2017**, *552*, 219.

(9) Patel, N.; Padera, R.; Sanders, G. H. W.; Cannizzaro, S. M.; Davies, M. C.; Langer, R.; Roberts, C. J.; Tendler, S. J. B.; Williams, P. M.; Shakesheff, K. M. Spatially Controlled Cell Engineering on Biodegradable Polymer Surfaces. *FASEB J.* **1998**, *12*, 1447–1454.

(10) Huang, J.; Gräter, S. V.; Corbellini, F.; Rinck, S.; Bock, E.; Kemkemer, R.; Kessler, H.; Ding, J.; Spatz, J. P. Impact of Order and Disorder in RGD Nanopatterns on Cell Adhesion. *Nano Lett.* **2009**, *9*, 1111–1116.

(11) Schvartzman, M.; Palma, M.; Sable, J.; Abramson, J.; Hu, X.; Sheetz, M. P.; Wind, S. J. Nanolithographic Control of the Spatial Organization of Cellular Adhesion Receptors at the Single-Molecule Level. *Nano Lett.* **2011**, *11*, 1306–1312.

(12) Cavalcanti-Adam, E. A.; Micoulet, A.; Blümmel, J.; Auernheimer, J.; Kessler, H.; Spatz, J. P. Lateral Spacing of Integrin Ligands Influences Cell Spreading and Focal Adhesion Assembly. *Eur. J. Cell Biol.* **2006**, *85*, 219–224.

(13) Delcassian, D.; Depoil, D.; Rudnicka, D.; Liu, M.; Davis, D. M.; Dustin, M. L.; Dunlop, I. E. Nanoscale Ligand Spacing Influences Receptor Triggering in T Cells and NK Cells. *Nano Lett.* **2013**, *13*, 5608–5614.

(14) Angers-Loustau, A.; Côté, J.-F.; Charest, A.; Dowbenko, D.; Spencer, S.; Lasky, L. A.; Tremblay, M. L. Protein Tyrosine Phosphatase-PEST Regulates Focal Adhesion Disassembly, Migration, and Cytokinesis in Fibroblasts. *J. Cell Biol.* **1999**, *144*, 1019–1031.

(15) Cavalcanti-Adam, E. A.; Volberg, T.; Micoulet, A.; Kessler, H.; Geiger, B.; Spatz, J. P. Cell Spreading and Focal Adhesion Dynamics Are Regulated by Spacing of Integrin Ligands. *Biophys. J.* **2007**, *92*, 2964–2974.

(16) Vogel, V.; Sheetz, M. Local Force and Geometry Sensing Regulate Cell Functions. *Nat. Rev. Mol. Cell Biol.* **2006**, *7*, 265–275.

(17) Dutta, P. K.; Zhang, Y.; Blanchard, A. T.; Ge, C.; Rushdi, M.; Weiss, K.; Zhu, C.; Ke, Y.; Salaita, K. Programmable Multivalent DNA-Origami Tension Probes for Reporting Cellular Traction Forces. *Nano Lett.* **2018**, *18*, 4803–4811.

(18) Lagarrigue, F.; Vikas Anekal, P.; Lee, H.-S.; Bachir, A. I.; Ablack, J. N.; Horwitz, A. F.; Ginsberg, M. H. A RIAM/Lamellipodin–Talin–Integrin Complex Forms the Tip of Sticky Fingers That Guide Cell Migration. *Nat. Commun.* **2015**, *6*, 8492.

(19) Bachir, A. I.; Zareno, J.; Moissoglu, K.; Plow, E. F.; Gratton, E.; Horwitz, A. R. Integrin-Associated Complexes Form Hierarchically with Variable Stoichiometry in Nascent Adhesions. *Curr. Biol.* **2014**, *24*, 1845–1853.

(20) Arnold, M.; Cavalcanti-Adam, E. A.; Glass, R.; Blümmel, J.; Eck, W.; Kantlehner, M.; Kessler, H.; Spatz, J. P. Activation of Integrin Function by Nanopatterned Adhesive Interfaces. *ChemPhysChem* **2004**, *5*, 383–388.

(21) Le Saux, G.; Edri, A.; Keydar, Y.; Hadad, U.; Porgador, A.; Schvartzman, M. Spatial and Chemical Surface Guidance of NK Cell Cytotoxic Activity. *ACS Appl. Mater. Interfaces* **2018**, *10*, 11486–11494.

(22) Cai, H.; Muller, J.; Depoil, D.; Mayya, V.; Sheetz, M. P.; Dustin, M. L.; Wind, S. J. Full Control of Ligand Positioning Reveals Spatial Thresholds for T Cell Receptor Triggering. *Nat. Nanotechnol.* **2018**, *13*, 610–617.

(23) Changede, R.; Cai, H.; Wind, S.; Sheetz, M. P. Ligand Geometry Controls Adhesion Formation *via* Integrin Clustering. *bioRxiv* **2018**, 435826.

(24) Graeter, S. V.; Huang, J.; Perschmann, N.; López-García, M.; Kessler, H.; Ding, J.; Spatz, J. P. Mimicking Cellular Environments by Nanostructured Soft Interfaces. *Nano Lett.* **2007**, *7*, 1413–1418.

(25) Cai, H.; Depoil, D.; Palma, M.; Sheetz, M. P.; Dustin, M. L.; Wind, S. J. Bifunctional Nanoarrays for Probing the Immune Response at the Single-Molecule Level. *J. Vac. Sci. Technol. B, Nanotechnol. Microelectron. Mater. Process. Meas. Phenom.* **2013**, *31*, 06F902.

(26) Rothemund, P. W. K. Folding DNA to Create Nanoscale Shapes and Patterns. *Nature* **2006**, *440*, 297–302.

(27) Hung, A. M.; Micheel, C. M.; Bozano, L. D.; Osterbur, L. W.; Wallraff, G. M.; Cha, J. N. Large-Area Spatially Ordered Arrays of Gold Nanoparticles Directed by Lithographically Confined DNA Origami. *Nat. Nanotechnol.* **2010**, *5*, 121–126.

(28) Zhang, F.; Nangreave, J.; Liu, Y.; Yan, H. Structural DNA Nanotechnology: State of the Art and Future Perspective. *J. Am. Chem. Soc.* **2014**, *136*, 11198–11211.

(29) Kearney, C. J.; Lucas, C. R.; O'Brien, F. J.; Castro, C. E. DNA Origami: Folded DNA-Nanodevices That Can Direct and Interpret Cell Behavior. *Adv. Mater.* **2016**, *28*, 5509–5524.

(30) Rinker, S.; Ke, Y.; Liu, Y.; Chhabra, R.; Yan, H. Self-Assembled DNA Nanostructures for Distance-Dependent Multivalent Ligand-Protein Binding. *Nat. Nanotechnol.* **2008**, *3*, 418–422.

(31) Shen, H.; Wang, Y.; Wang, J.; Li, Z.; Yuan, Q. Emerging Biomimetic Applications of DNA Nanotechnology. *ACS Appl. Mater. Interfaces* **2018**, Article ASAP, DOI: 10.1021/acsami.8b06175.

(32) Li, S.; Jiang, Q.; Liu, S.; Zhang, Y.; Tian, Y.; Song, C.; Wang, J.; Zou, Y.; Anderson, G. J.; Han, J.-Y.; Chang, Y.; Liu, Y.; Zhang, C.; Chen, L.; Zhou, G.; Nie, G.; Yan, H.; Ding, B.; Zhao, Y.; A DNA Nanorobot Functions as a Cancer Therapeutic in Response to a Molecular Trigger *in Vivo*. *Nat. Biotechnol.* **2018**, *36*, 258–264.

(33) Huang, D.; Freeley, M.; Palma, M. DNA-Mediated Patterning of Single Quantum Dot Nanoarrays: A Reusable Platform for Single-Molecule Control. *Sci. Rep.* **2017**, *7*, 45591.

(34) Parsons, J. T.; Parsons, S. J. Src Family Protein Tyrosine Kinases: Cooperating with Growth Factor and Adhesion Signaling Pathways. *Curr. Opin. Cell Biol.* **1997**, *9*, 187–192.

(35) Bill, H. M.; Knudsen, B.; Moores, S. L.; Muthuswamy, K.; Rao, V. R.; Brugge, J. S.; Miranti, K.; Muthuswamy, S. K.; Miranti, C. K. Epidermal Growth Factor Receptor-Dependent Regulation of Integrin-Mediated Signaling and Cell Cycle Entry in Epithelial

Cells Epidermal Growth Factor Receptor-Dependent Regulation of Integrin-Mediated Signaling and Cell Cycle Entry in Epithelial Cells. *Society* **2004**, *24*, 8586–8599.

(36) Kim, S. H.; Turnbull, J.; Guimond, S. Extracellular Matrix and Cell Signalling: The Dynamic Cooperation of Integrin, Proteoglycan and Growth Factor Receptor. *J. Endocrinol.* **2011**, *209*, 139–151.

(37) Saha, A.; Ellison, D.; Thomas, G. J.; Vallath, S.; Mather, S. J.; Hart, I. R.; Marshall, J. F. High-Resolution *in Vivo* Imaging of Breast Cancer by Targeting the pro-Invasive Integrin Alphavbeta6. *J. Pathol.* **2010**, *222*, 52–63.

(38) DiCara, D.; Rapisarda, C.; Sutcliffe, J. L.; Violette, S. M.; Weinreb, P. H.; Hart, I. R.; Howard, M. J.; Marshall, J. F. Structure-Function Analysis of Arg-Gly-Asp Helix Motifs in Avβ6 Integrin Ligands. *J. Biol. Chem.* **2007**, *282*, 9657–9665.

(39) Caswell, P. T.; Chan, M.; Lindsay, A. J.; McCaffrey, M. W.; Boettiger, D.; Norman, J. C. Rab-Coupling Protein Coordinates Recycling of A5β1 Integrin and EGFR1 to Promote Cell Migration in 3D Microenvironments. *J. Cell Biol.* **2008**, *183*, 143–155.

(40) Reginato, M. J.; Mills, K. R.; Paulus, J. K.; Lynch, D. K.; Sgroi, D. C.; Debnath, J.; Muthuswamy, S. K.; Brugge, J. S. Integrins and EGFR Coordinately Regulate the Pro-Apoptotic Protein Bim to Prevent Anoikis. *Nat. Cell Biol.* **2003**, *5*, 733–740.

(41) Paul, N. R.; Jacquemet, G.; Caswell, P. T. Endocytic Trafficking of Integrins in Cell Migration. *Curr. Biol.* **2015**, *25*, R1092–R1105.

(42) Mitra, S. K.; Schlaepfer, D. D. Integrin-Regulated FAK–Src Signaling in Normal and Cancer Cells. *Curr. Opin. Cell Biol.* **2006**, *18*, 516–523.

(43) Streuli, C. H.; Akhtar, N. Signal Co-Operation between Integrins and Other Receptor Systems. *Biochem. J.* **2009**, *418*, 491–506.

(44) The linear structure of A20FMDV2 peptide is stable in many conditions including wide arrange of pH and temperature. The peptide remains functional even when heated up to 97°C making it possible to apply A20FMDV2 in many approaches including thermal synthesis.

(45) Huang, D.; Freeley, M.; Palma, M. Single-Molecule Patterning *via* DNA Nanostructure Assembly: A Reusable Platform. Methods Mol. Biol. 2018, 1811, 231–251.

(46) Jaehrling, S.; Thelen, K.; Wolfram, T.; Pollerberg, G. E. Nanopatterns Biofunctionalized with Cell Adhesion Molecule DM-GRASP Offered as Cell Substrate: Spacing Determines Attachment and Differentiation of Neurons. *Nano Lett.* **2009**, *9*, 4115–4121.

(47) Tummers, W. S.; Farina-Sarasqueta, A.; Boonstra, M. C.; Prevoo, H. A.; Sier, C. F.; Mieog, J. S.; Morreau, J.; van Eijck, C. H.; Kuppen, P. J.; van de Velde, C. J.; Bonsing, B. A.; Vahrmeijer, A. L.; Swijnenburg, R.-J. Selection of Optimal Molecular Targets for Tumor-Specific Imaging in Pancreatic Ductal Adenocarcinoma. *Oncotarget* **2017**, *8*, 56816–56828.

(48) Wang, F.; Weaver, V. M.; Petersen, O. W.; Larabell, C. A.; Dedhar, S.; Briand, P.; Lupu, R.; Bissell, M. J. Reciprocal Interactions between B1-Integrin and Epidermal Growth Factor Receptor in Three-Dimensional Basement Membrane Breast Cultures: A Different Perspective in Epithelial Biology. *Proc. Natl. Acad. Sci.* **1998**, *95*, 14821–14826.

(49) Moro, L. Integrins Induce Activation of EGF Receptor: Role in MAP Kinase Induction and Adhesion-Dependent Cell Survival. *EMBO J*. **1998**, *17*, 6622–6632.

(50) Mammen, M.; Choi, S.-K.; Whitesides, G. M. Polyvalent Interactions in Biological Systems: Implications for Design and Use of Multivalent Ligands and Inhibitors. *Angew. Chemie Int. Ed*. **1998**, *37*, 2754–2794.

(51) Kiessling, L. L.; Gestwicki, J. E.; Strong, L. E. Synthetic Multivalent Ligands as Probes of Signal Transduction. *Angew. Chemie Int. Ed*. **2006**, *45*, 2348–2368.

(52) Bhatia, S.; Camacho, L. C.; Haag, R. Pathogen Inhibition by Multivalent Ligand Architectures. *J. Am. Chem. Soc*. **2016**, *138*, 8654–8666.

TOC graphic